198692: garnet–staurolite-bearing chloritoid semipelitic schist, Chittering belt

(South West Terrane, Yilgarn Craton)

Kelsey, DE, Blereau, ER, Korhonen, FJ and Romano, SS

Location and sampling

Moora (SH 50-10), Moora (2136)

MGA Zone 50, 408600E 6576000N

Warox Site FJKBGD198692

Sampled on 17 June 2010

This sample was collected from rock cobbles in a creek 46 km north-northeast of Gingin, 3.1 km west-southwest of Gillingarra Hill and 2 km south-southwest of the Gillingarra Road – Bindoon – Moora Road junction, with cobbles likely sourced from hills immediately west. The sample was collected as part of the Geological Survey of Western Australia's (GSWA) 2003–14 Yilgarn Craton Metamorphic Project, and referred to in that study as sample BG10-74j. The results from this project have not been released by GSWA, although select data have been published in Goscombe et al. (2019).

Geological context

The unit sampled is a semipelitic schist from the western margin of the South West Terrane of the Yilgarn Craton (Cassidy et al., 2006; Quentin de Gromard et al., 2021), at the boundary between the northern end of the informally named Chittering and Jimperding metamorphic belts and within the Darling Fault Zone system (Wilde, 1994, 2001). The South West Terrane consists of mainly metasedimentary rocks, migmatite and gneiss (Wilde, 1994; Quentin de Gromard et al., 2021). Granitic and gneissic rocks along the western margin have yielded U–Pb zircon dates of 2.68 – 2.61 Ga (e.g. Nelson, 2004; Nemchin and Pidgeon, 1997; Lu et al., 2015a, 2019). Monazite U–Pb age data from a semipelitic schist collected from the same locality as the sample reported here, gives a spread of dates from c. 735 to 662 Ma, interpreted as dating the timing of metamorphism (GSWA 198694, preliminary data). A semipelitic gneiss sample 255 km south along the Darling Fault Zone records a U–Pb zircon metamorphic date of 707 ± 5 Ma (GSWA 198532, Wingate et al., 2014). Monazite U–Pb age data from the same sample yields a spread of dates from c. 902 to 640 Ma, and possibly three age components at c. 860, 724 and 668 Ma within that spread that are tentatively interpreted as either the ages of separate hydrothermal or metamorphic events, or loss of radiogenic Pb (GSWA 198532, Fielding et al., 2021). Single-grain biotite $^{40}Ar/^{39}Ar$ age data decrease abruptly westwards from c. 2580 to 2480 Ma across most of the Yilgarn Craton to 1100–1000 Ma over a narrow transitional zone (30–40 km wide), and reach 630–620 Ma along the western margin of the craton (Lu et al., 2015b).

Petrographic description

The sample is a semipelitic schist (Fig. 1) containing 71% quartz, 10% muscovite, 7% biotite, 7% chloritoid, 3% garnet, 2% chlorite, 0.2% staurolite and trace amounts of ilmenite, xenotime and monazite (Fig. 2; Table 1). The sample has a quartz-rich matrix (up to 0.5 mm in diameter) with a well-defined foliation (Figs 1, 2) of predominantly quartz, muscovite (up to 0.5 mm) and lesser biotite (up to 0.25 mm), and mica-poor layers rich in porphyroblastic chloritoid (0.25 – 10 mm in length) and quartz. Quartz has an inequigranular–polygonal to granoblastic texture and has internal subgrains. A 1.2 cm long, high aspect ratio (6:1) garnet porphyroblast occurs within a chloritoid-bearing layer, and the two minerals are in direct contact (Figs 2, 3). Quartz and rare ilmenite occur as inclusions in chloritoid. Quartz and rare chloritoid occur as inclusions in garnet. Fractures through garnet are perpendicular to the foliation and filled with chlorite (Figs 2, 3). Rare porphyroblasts of staurolite, 2–3 mm in diameter, with inclusions of quartz and an aspect ratio of 2:1, are wrapped by the foliation. Staurolite occurs distant from garnet and chloritoid and

one grain is distinctly more ovoid shaped than garnet and chloritoid (Figs 2, 3). Biotite occurs as strongly aligned, acicular grains as well as less well oriented, more anhedral grains. Chlorite is most common along fractures through garnet. It is rare as a matrix mineral aligned along foliation and it also occurs as rare aggregates marginal to porphyroblastic minerals. Ilmenite is spatially associated with chloritoid and less than 100 μm in size. The sample is iron-stained with likely Fe-hydroxides and these are most abundant in fractures in garnet and chloritoid.

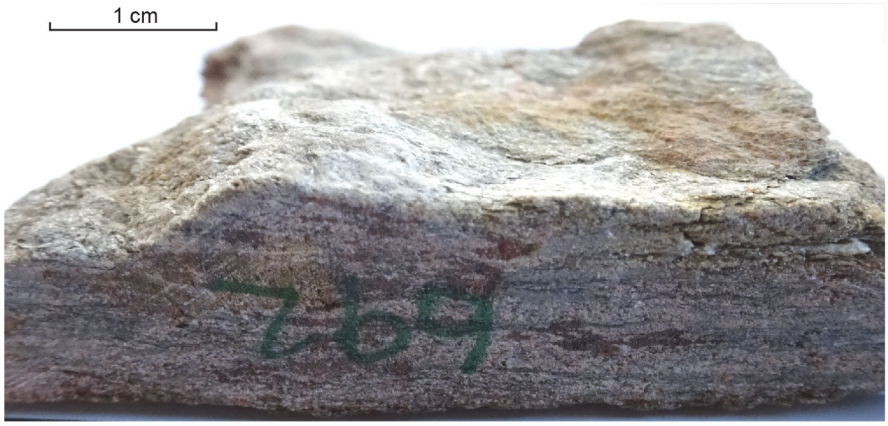

Figure 1. **Hand specimen image of sample 198692: garnet–staurolite-bearing chloritoid semipelitic schist, Chittering belt**

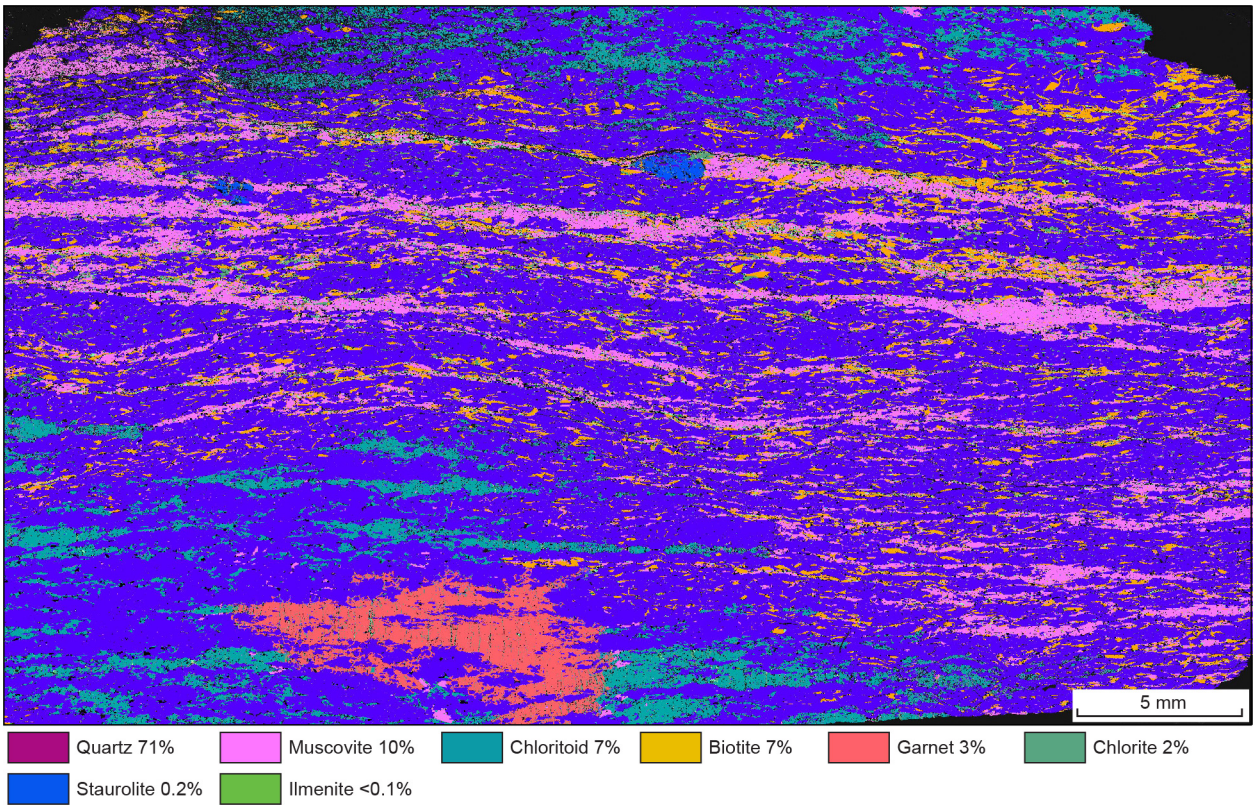

Figure 2. **TESCAN Integrated Mineral Analyser (TIMA) image of an entire thin section from sample 198692: garnet–staurolite-bearing chloritoid semipelitic schist, Chittering belt. Volume percent proportion of major rock-forming minerals are calculated by the TIMA software**

Table 1. Mineral modes for sample 198692: garnet–staurolite-bearing chloritoid semipelitic schist, Chittering belt

Mineral modes	*Qz*	*Ms*	*Bt*	*Ctd*	*Grt*	*Chl*	*St*	*Ilm*
Observed (vol%)[(a)]	71	10	7	7	3	2	0.20	<0.1
Predicted (mol%)								
@ 380 °C, 4.2 kbar	62	12	14	5	1	–	6.0	<0.1
@ 490 °C, 8.6 kbar	60	18	7	7	7	–	<0.1	<0.1

NOTES: (a) trace xenotime and monazite also present in thin section. No apatite occurs.
– not present

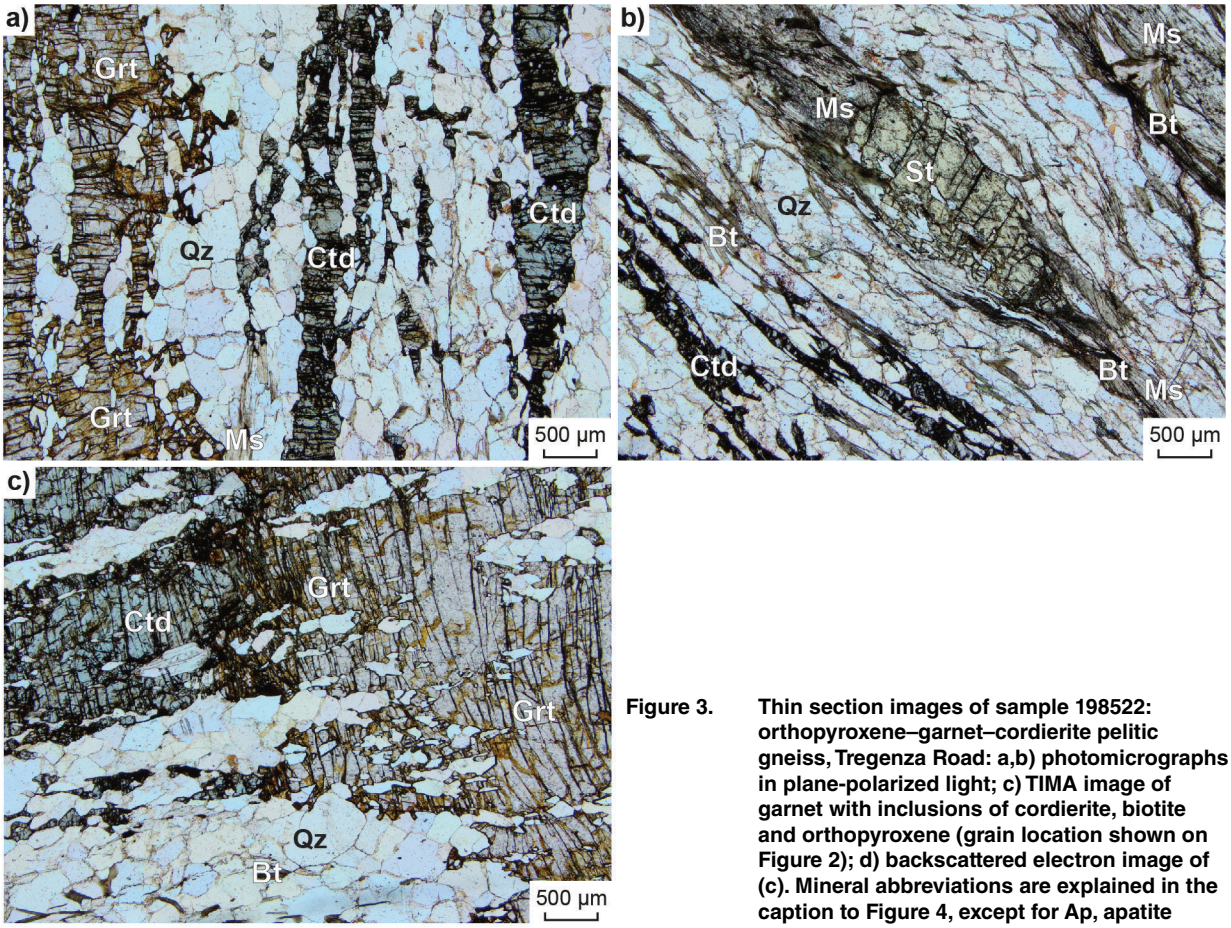

Figure 3. Thin section images of sample 198522: orthopyroxene–garnet–cordierite pelitic gneiss, Tregenza Road: a,b) photomicrographs in plane-polarized light; c) TIMA image of garnet with inclusions of cordierite, biotite and orthopyroxene (grain location shown on Figure 2); d) backscattered electron image of (c). Mineral abbreviations are explained in the caption to Figure 4, except for Ap, apatite

Analytical details

Preliminary *P–T* estimates were obtained using multiple-reaction thermobarometry calculated from the mineral compositions (Table 2; Goscombe et al., 2015). These estimates were derived from the 'averagePT' module (avPT) in the program THERMOCALC version tc325 (Powell and Holland, 1988), using the internally consistent Holland and Powell (1998) dataset.

The metamorphic evolution of this sample has subsequently been re-evaluated using phase equilibria modelling, based on the bulk rock composition (Table 3). The bulk-rock composition was determined by X-ray fluorescence spectroscopy, together with loss on ignition (LOI). The modelled O content (for Fe^{3+}) was constrained to be equal to 2% of FeOT via exploration of calculated phase equilibria at different oxidation states prior to calculation of the *P–T* pseudosection. The measured LOI amount is too high and did not allow for prediction of the interpreted peak mineral assemblage. Exploration with calculated phase equilibria at different hydration states (and 2% oxidation state as per above) prior to calculation of the *P–T* pseudosection constrained a drier hydration state as being suitable for use as the amount of H_2O.

Thermodynamic calculations were performed in the MnNCKFMASHTO ($MnO–Na_2O–CaO–K_2O–FeO–MgO–Al_2O_3–SiO_2–H_2O–TiO_2–O$) system using THERMOCALC version tc340 (updated October 2013; Powell and Holland 1988) and the internally consistent thermodynamic dataset of Holland and Powell (2011; dataset tc-ds62, created in February 2012). The activity–composition relations used in the modelling are detailed in White et al. (2014a,b). Additional information on the workflow with relevant background and methodology are provided in Korhonen et al. (2020).

Table 2. Measured whole-rock and modelled compositions for sample 1198692: semipelitic schist, Chittering belt

XRF whole-rock composition (wt%)[a]												
SiO_2	**TiO_2**	**Al_2O_3**	**Fe_2O_3**	**FeO[b]**	**MnO**	**MgO**	**CaO**	**Na_2O**	**K_2O**	**P_2O_5**	**LOI**	**Total**
73.00	0.23	11.70	–	6.98	0.07	1.20	0.10	0.18	2.47	0.02	2.22	98.17
Normalized composition used for phase equilibria modelling (mol%)												
SiO_2	**TiO_2**	**Al_2O_3**	**O[c]**	**FeO^T[d]**	**MnO**	**MgO**	**CaO**	**Na_2O**	**K_2O**	**–**	**H_2O[e]**	**Total**
77.20	0.19	7.29	0.06	6.17	0.06	1.90	0.08	0.19	1.66		5.20	100

NOTES: (a) Data from Goscombe et al. (2015)
(b) FeO content is total Fe
(c) O content (for Fe_2O_3) constrained to be 2% of total Fe
(d) FeO^T = moles FeO + 2 * moles O
(e) H_2O content constrained by phase equilibria modelling prior to calculation of the *P–T* pseudosection

Results

Metamorphic *P–T* estimates (± 2σ uncertainty) calculated using multiple-reaction thermobarometry are 7.0 ± 1.1 kbar and 563 ± 8 °C (Goscombe et al., 2015). These calculations used the rim and matrix mineral compositions (Table 2) to estimate peak conditions.

The *P–T* pseudosection for this sample was calculated over the range 3–12 kbar and 300–600 °C (Fig. 4). Garnet is stable everywhere except for a small field (labelled D) below 3.4 kbar at about 530–590 °C. Staurolite is stable below about 8.8 kbar, and chloritoid is stable at temperatures less than about 450–520 °C at all pressures. Kyanite is stable in a triangular-shaped region between about 6.7 to 10.3 kbar and <300 to 370 °C. Chlorite stabilizes up-temperature at the expense of chloritoid, in the window ~430 to >600 °C, but destabilizes over the interval ~530–600 °C due to the stability of free water with increasing temperature. Glaucophane is stable in the top left part of the pseudosection above about 5.5 kbar at 300 °C and above about 11.5 kbar at 480 °C. Amphibole with a hornblende–grunerite solid solution composition is stable below about 4.6 kbar at 480 °C. Plagioclase is stable below about 4.2 kbar at 540 °C. Albite is stable below about 375 °C at 3 kbar. Ilmenite is stable across much of the pseudosection except for at high-pressure–low-temperature where rutile is stable instead and at the bottom right-hand corner. The calculated mineral modes (molar proportions approximately equivalent to vol%) of glaucophane, hornblende, plagioclase and albite are all about ≤1 mol%.

Interpretation

Based on the coarser grain size and mineral associations that support textural equilibrium, the peak metamorphic assemblage is interpreted to be biotite–garnet–staurolite–chloritoid–ilmenite–muscovite–quartz. It is unclear if the peak metamorphic mineral assemblage includes all three of garnet, chloritoid and staurolite as staurolite never occurs proximal to or in contact with garnet and chloritoid. However, the calculated phase equilibria results show that these three porphyroblastic minerals can stably coexist over a reasonably large *P–T* range of about 4.0 – 8.9 kbar and 340–505 °C (Fig. 4). As such, we interpret that these three minerals probably did stably coexist. These results yield lower temperatures and similar pressures to the estimates derived from conventional thermobarometry by Goscombe et al. (2015). Alternatively, the staurolite-absent assemblage biotite–garnet–chloritoid–ilmenite–muscovite–quartz occurs between 8.9 and 11.4 kbar, over the temperature range 395–500 °C, which could also be interpreted as the potential peak mineral assemblage. This interpretation implies that staurolite was not in equilibrium with garnet and chloritoid, which is difficult to resolve as these minerals are not observed in direct contact. The peak mineral assemblage is bound by the stability of hornblende at lower pressures, chlorite at higher temperatures, glaucophane at higher pressures and albite at lower temperatures. However, as the calculated modes of glaucophane, albite and hornblende are all ≤1 mol%, the predicted stability of these minerals provide only weak constraints on the limits of the peak mineral assemblage field.

Compositional zoning within garnet from near-identical semipelitic schist sample GSWA 198694 shows a decrease in CaO, MnO and FeO and an increase in MgO from core to rim (Appendix 1). Such trends are typical for prograde growth zoning. Zoning in Mn (spessartine) in particular shows that garnet growth occurred in an active strain field, its growing shape constrained by the synchronously-developing mylonitic fabric. Most or all chlorite is interpreted as retrograde due to its textural occurrence predominantly within fractures. These fractures through garnet probably have chemical zoning about them as comparable sample GSWA 198694, collected from the same locality and having almost identical mineralogy and high-strain foliation, shows such a feature, particularly in Fe and Mg, showing that the growth of retrograde chlorite affected the local chemical composition of garnet (Appendix 1). The occurrence of late chlorite and the possible presence of some late biotite provide only loose constraints on the trajectory of the *P–T* path as chlorite occurs up-temperature from the peak assemblage field and it is not clear if the retrogression involved fluid ingress that would change the bulk-composition that was used in the modelling. It is unclear how the spread of monazite age data (c. 735 to 662 Ma) from the comparable sample GSWA 198694 (preliminary data) relates in detail to the metamorphic parageneses documented here, but some of the spread may be related to variable Pb-loss during one event induced by strain/mylonitization. The thermal regime for peak *P–T* conditions (e.g. Stüwe, 2007; Korhonen et al., 2020) defines low apparent thermal gradients of ~45–95 °C/kbar. Extending peak conditions to include the staurolite-absent assemblage at higher pressures ('Bt Grt Ctd Ilm' field on Figure 4) results in even lower apparent thermal gradients.

Based on the assumption that garnet, chloritoid and staurolite were in equilibrium, peak metamorphic conditions are estimated at 4.0 – 8.9 kbar and 340–505 °C, with an apparent thermal gradient between 45 and 95 °C/kbar.

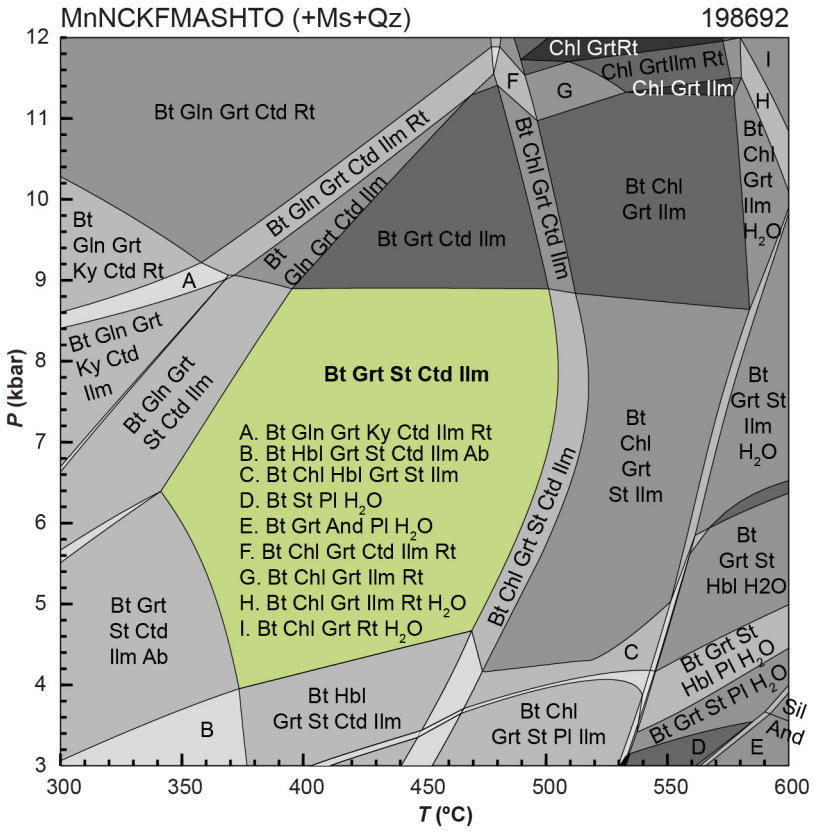

Figure 4. ***P–T*** **pseudosection calculated for sample 198692: garnet–staurolite-bearing chloritoid semipelitic schist, Chittering belt. Assemblage fields corresponding to peak metamorphic conditions are shown in bold text and pale green shading. Abbreviations: Ab, albite; And, andalusite; Bt, biotite; Chl, chlorite; Ctd, chloritoid; Gln, glaucophane; Grt, garnet; H_2O, aqueous fluid (pure H_2O); Hbl, hornblende; Ilm, ilmenite; Ky, kyanite; Ms, muscovite; Pl, plagioclase; Qz, quartz; Rt, rutile; Sil, sillimanite; St, staurolite**

References

Cassidy, KF, Champion, DC, Krapež, B, Barley, ME, Brown, SJA, Blewett, RS, Groenewald, PB and Tyler, IM 2006, A revised geological framework for the Yilgarn Craton, Western Australia: Geological Survey of Western Australia, Record 2006/8, 8p.

Droop, GTR 1987, A general equation for estimating Fe3+ concentrations in ferromagnesian silicates and oxides from microprobe analyses, using stoichiometric criteria: Mineralogical Magazine, v. 51, no. 361, p. 431–435.

Fielding, IOH, Wingate, MTD, Korhonen, FJ and Rankenburg, K 2021, 198532: semipelitic gneiss, Brunswick River; Geochronology Record 1771: Geological Survey of Western Australia, 5p.

Goscombe, B, Blewett, R, Groenewald, PB, Foster, D, Wade, B, Wyche, S, Wingate, MTD and Kirkland, CL 2015, Metamorphic Evolution of the Yilgarn Craton: Geological Survey of Western Australia (unpublished), 910p.

Goscombe, B, Foster, DA, Blewett, R, Czarnota, K, Wade, B, Groenewald, B and Gray, D 2019, Neoarchaean metamorphic evolution of the Yilgarn Craton: a record of subduction, accretion, extension and lithospheric delamination: Precambrian Research, article no. 105441, doi:10.1016/j.precamres.2019.105441.

Holland, TJB and Powell, R 1998, An internally consistent thermodynamic data set for phases of petrological interest: Journal of Metamorphic Geology, v. 16, no. 3, p. 309–343.

Holland, TJB and Powell, R 2011, An improved and extended internally consistent thermodynamic dataset for phases of petrological interest, involving a new equation of state for solids: Journal of Metamorphic Geology, v. 29, no. 3, p. 333–383.

Korhonen, FJ, Kelsey, DE, Fielding IOH and Romano, SS 2020, The utility of the metamorphic rock record: constraining the pressure–temperature–time conditions of metamorphism: Geological Survey of Western Australia, Record 2020/14, 24p.

Lu, S, Phillips, D, Kohn, BP, Gleadow, AJW and Matchan, EL 2015b, Thermotectonic evolution of the western margin of the Yilgarn craton, Western Australia: New insights from 40Ar/39Ar analysis of muscovite and biotite: Precambrian Research, v. 270, p. 139–154, doi:10.1016/j.precamres.2015.09.014.

Lu, Y, Wingate, MTD, Bodorkos, S and Wyche, S 2015a, 184115: granite gneiss, Kirup; Geochronology Record 1279: Geological Survey of Western Australia, 4p.

Lu, Y, Wingate, MTD and Smithies, RH 2019, 224368: metagranodiorite, Kingsbury Drive; Geochronology Record 1586: Geological Survey of Western Australia, 4p.

Nelson, DR 2004, 169079: biotite granodiorite gneiss, Harvey Dam intake tower; Geochronology Record 114: Geological Survey of Western Australia, 5p.

Nemchin, AA and Pidgeon, RT 1997, Evolution of the Darling Range Batholith, Yilgarn Craton, Western Australia: a SHRIMP study: Journal of Petrology, v. 38, p. 625–649.

Powell, R and Holland, TJB 1988, An internally consistent dataset with uncertainties and correlations: 3. Applications to geobarometry, worked examples and a computer program: Journal of Metamorphic Geology, v. 6, no. 2, p. 173–204.

Quentin de Gromard, R, Ivanic, TJ and Zibra, I 2021, Pre-Mesozoic interpreted bedrock geology of the southwest Yilgarn, 2021, *in* Accelerated Geoscience Program extended abstracts: Geological Survey of Western Australia, Record 2021/4, p. 122–144.

Stüwe, K 2007, Geodynamics of the lithosphere: An introduction: Springer, Berlin, 493p.

White, RW, Powell, R, Holland, TJB, Johnson, TE and Green, ECR 2014a, New mineral activity–composition relations for thermodynamic calculations in metapelitic systems: Journal of Metamorphic Geology, v. 32, no. 3, p. 261–286.

White, RW, Powell, R and Johnson, TE 2014b, The effect of Mn on mineral stability in metapelites revisited: New a–x relations for manganese-bearing minerals: Journal of Metamorphic Geology, v. 32, no. 8, p. 809–828.

Wilde, SA 1994, Crustal evolution of the southwestern Yilgarn Craton: Geological Society of Australia (Western Australia Division), Excursion Guidebook 7, 20p.

Wilde, SA 2001, Jimperding and Chittering metamorphic belts, Western Australia — a field guide: Geological Survey of Western Australia, Record 2001/12, 24p

Wingate, MTD, Kirkland, CL, Goscombe, B and Wyche, S 2014, 198532: pelitic gneiss, Brunswick River; Geochronology Record 1214: Geological Survey of Western Australia, 7p.

Links

Metamorphic history introduction document: Intro_2020.pdf

Appendix

Quantitative EPMA compositional maps for near-identical semipelitic schist sample GSWA 198694, collected from the same locality. Maps were analysed by wavelength-dispersive spectroscopy (WDS), and calculated for proportion of garnet end-members. Grossular, Ca = (Fe^{2+} + Mg + Mn + Ca); Pyrope, Mg = (Fe^{2+} + Mg + Mn + Ca); Almandine, Fe^{2+} = (Fe^{2+} + Mg + Mn + Ca); Spessartine, Mn = (Fe^{2+} + Mg + Mn + Ca)

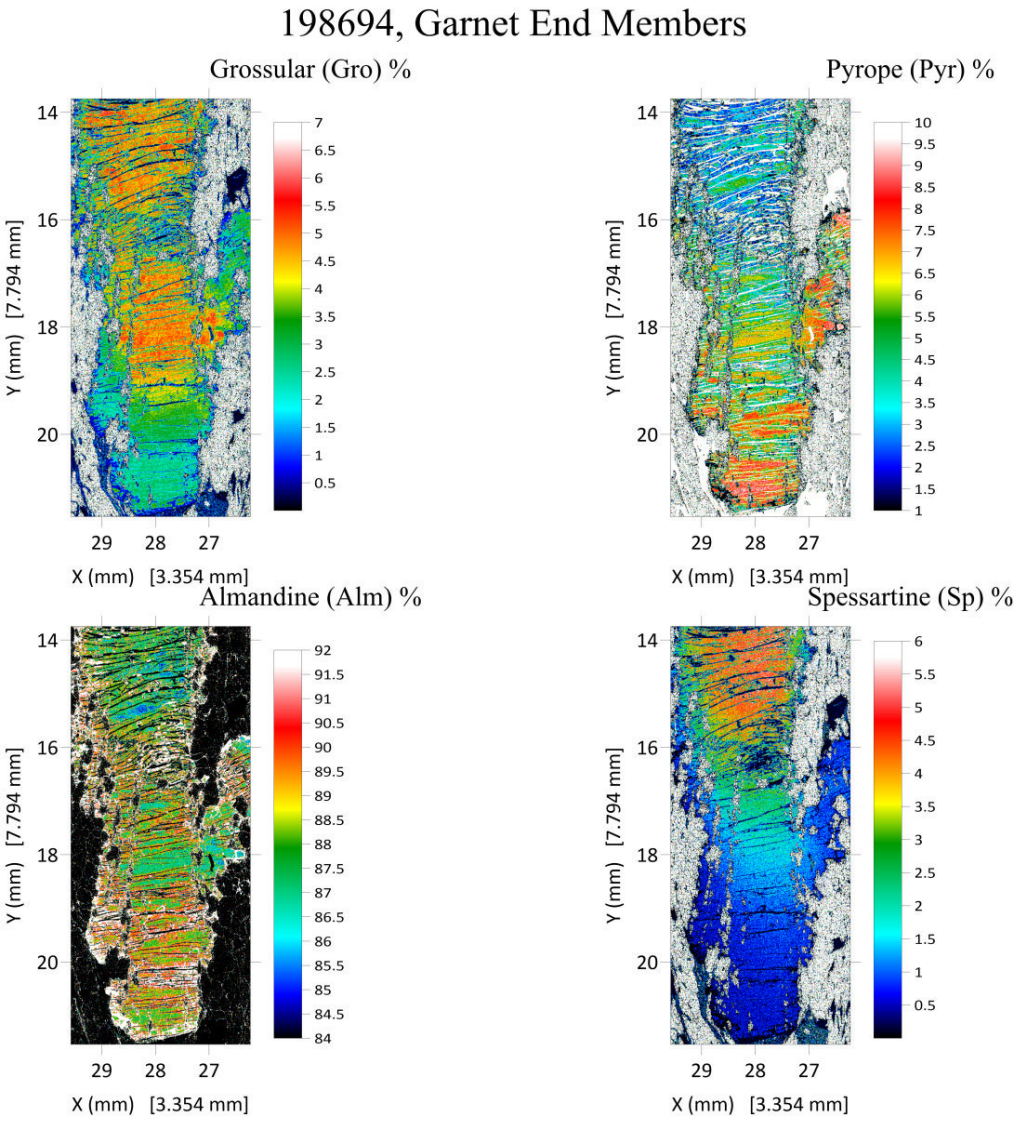

Recommended reference for this publication

Kelsey, DE, Blereau, ER, Korhonen, FJ and Romano, SS 2022, 198692: garnet–staurolite-bearing chloritoid semipelitic schist, Chittering belt; Metamorphic History Record 16: Geological Survey of Western Australia, 8p.

Data obtained: 22 November 2021

Date released: 14 April 2022

This Metamorphic History Record was last modified on 29 March 2022.

Grid references in this publication refer to the Geocentric Datum of Australia 1994 (GDA94). All locations are quoted to at least the nearest 100 m.

WAROX is GSWA's field observation and sample database. WAROX site IDs have the format 'ABCXXXnnnnnnSS', where ABC = geologist username, XXX = project or map code, nnnnnn = 6 digit site number, and SS = optional alphabetic suffix (maximum 2 characters).

Isotope and element analyses are routinely conducted using the GeoHistory laser ablation ICP-MS and Sensitive High-Resolution Ion Microprobe (SHRIMP) ion microprobe facilities at the John de Laeter Centre (JdLC), Curtin University, with the financial support of the Australian Research Council and AuScope National Collaborative Research Infrastructure Strategy (NCRIS). The TESCAN Integrated Mineral Analyser (TIMA) instrument was funded by a grant from the Australian Research Council (LE140100150) and is operated by the JdLC with the support of the Geological Survey of Western Australia, The University of Western Australia (UWA) and Murdoch University. Mineral analyses are routinely obtained using the electron probe microanalyser (EPMA) facilities at the Centre for Microscopy, Characterisation and Analysis at UWA, and at Adelaide Microscopy, University of Adelaide.

Digital data related to WA Geology Online, including geochronology and digital geology, are available online at the Department's Data and Software Centre and may be viewed in map context at GeoVIEW.WA.

Further details of geoscience products are available from:
Information Centre
Department of Mines, Industry Regulation and Safety
100 Plain Street
EAST PERTH WA 6004
Telephone: +61 8 9222 3459 | Email: publications@dmirs.wa.gov.au
www.dmirs.wa.gov.au/GSWApublications